Key Points:
- A simple and fast method for electromagnetic material characterization based on an improved Fabry-Pérot technique is presented
- Simple criteria for the applicability of the method and an automatic procedure for the determination of the method's results are proposed
- The method is applied to several building materials to assess its applicability and accuracy: Results show a good accuracy level

Improved Fabry-Pérot Electromagnetic Material Characterization: Application and Results

L. Possenti[1] , J. Pascual-García[2] , V. Degli-Esposti[1] , A. Lozano-Guerrero[2] , M. Barbiroli[1] , M. T. Martinez-Inglés[3] , F. Fuschini[1] , J. V. Rodríguez[2] , E. M. Vitucci[1] , and J. M. Molina-García-Pardo[2]

[1]Department of Electrical, Electronic and Information Engineering "Guglielmo Marconi" (DEI), University of Bologna, Bologna, Italy, [2]Departamento Tecnologías de la Información y las Comunicaciones, Universidad Politécnica de Cartagena, Cartagena, Spain, [3]San Javier, Air Force Base, Ministerio de Defensa, UPCT, University Center of Defense, Murcia, Spain

Abstract While several mm-wave and sub-THz frequency bands are being proposed for next generation wireless systems to meet the increasing traffic demand, the electromagnetic properties of many common use materials at those frequencies still need to be determined. The evaluation of such properties is important for the design and deployment of future wireless networks. Recently, a simple method based on Fabry-Pérot resonance has been proposed to address the need of easy material characterization at mm-wave frequencies. In this study, the method has been improved and applied to the characterization of several materials at mm-wave and sub-THz frequencies, in order to assess its reliability, usability, and accuracy in practical cases. The method is shown to achieve a good accuracy level despite the very simple measurement setup and the great flexibility. However, some application limitations are highlighted and discussed in the paper. A method for electromagnetic material characterization based on an improved Fabry-Pérot technique is presented.

1. Introduction

Due to the congestion of the sub-6 GHz spectrum and to the necessity of finding large contiguous spectrum blocks for multigigabit applications, the use of several new frequency bands in the mm-wave and sub-THz (100–300 GHz) frequency range is being proposed worldwide (Elayan et al., 2020; Rappaport et al., 2019). With respect to sub-6 GHz bands, such frequencies generally show peculiar propagation characteristics and in particular higher diffraction and penetration losses from walls and objects that strongly depend on the different material parameters (Rappaport et al., 2019; Salous et al., 2016). Therefore, simple and fast electromagnetic characterization of construction and furniture materials at multiple frequency bands will soon become an urgent need for the design of future wireless networks and of smart buildings where such networks will have to operate. Material characterization is also necessary to properly use the increasingly popular deterministic simulation tools such as ray tracing.

Several methods for measuring the complex permittivity of materials have been developed over the years, including transmission line methods (Boughriet et al., 1997), coaxial probe methods (Canós Marín et al., 2013), resonant methods (Hirvonen et al., 1996; Works et al., 1944), and free space methods (Ghodgaonkar et al., 1989; Redheffer, 1947). Due to the possibility of measuring *effective* electromagnetic parameters of compound materials, free space methods are widely used as can be derived from 30 years literature analysis (B. R. Rao, 1989, D. K. Ghodgaonkar et al., 1990 to cite two of the oldest works and M. S. Hilario et al., 2019, A. A. Politiko et al., 2019, and H. Manh Cuong et al., 2017 to cite two of the most recent works related to the topic). Moreover, free space methods do not require to cut or machine the sample in order to measure it and therefore are suitable for nondestructive tests on large construction and furnishing material samples. However, conventional free-space methods usually need accurate reflection or transmission measurements for different incidence/reception angles that require rotating positioners, an anechoic environment, and complex maximum-likelihood parameter determination methods or the numerical solution of scattering equations.

Recently, a simple and fast method for the characterization of low-loss materials based on the Fabry-Pérot (FP) resonance that takes place inside a material slab has been proposed (Degli-Esposti et al., 2017).

Instead of performing multiple measurements, a wide measurement bandwidth is used to extract the same information from the difference between adjacent resonance frequencies, using a simple, fixed setup with a Spectrum Analyzer (SA) or a Vector Network Analyzer (VNA). Because of the simplicity of the setup, measurements can even be carried out on site, without the need of carrying around heavy or large material samples such as a marble slab or a door leaf. However, the method—as any other characterization method—has its limitations: It can only be applied to thick enough, with respect to the wavelength, slabs, and/or over a wide enough bandwidth in order to show up at least two to three successive resonance dips on the frequency span. At mm-wave frequencies, a thickness of 1 cm and a bandwidth of 1–2 GHz are usually enough to successfully apply the method: Over such a bandwidth the complex permittivity of most materials at frequencies above 6 GHz is generally constant. Moreover, it can only be applied to materials that can be considered relatively homogeneous: This means that for grainy materials such as sandstone or chipboard, grains must be significantly smaller than the wavelength in order to prevent severe diffuse scattering from hampering FP resonance. These problems are further discussed in sections 2 and 3 where criteria for the method's applicability are also provided. While the application of the method to sub-6 GHz frequencies would require too thick material samples and at THz frequencies would suffer in case of grainy materials with grain dimensions comparable or larger than the wavelength, the method appears quite suitable for most building materials at mm-wave and sub-THz frequencies.

The method was first proposed in Degli-Esposti et al. (2017), and its application to a few construction materials was demonstrated therein. A refinement of the method for what concerns the evaluation of the imaginary part of the complex permittivity was presented in Possenti et al. (2020).

The contribution of the present work is fourfold. First of all, the method is further developed to determine an automatic procedure for the evaluation of the interresonance frequency distance and of the insertion loss. Second, the use of time gating to clean up the frequency response and improve performance is introduced and discussed. Third, the application of the method to grainy material is discussed: An a priori criterium for the applicability of the method based on the ratio of grain size to the wavelength as well an a posteriori criterion for the verification of the results based on the resonance Q-factor are provided. Finally, the method is applied for the first time to the characterization of several materials using both fixed and portable setups at different mm-wave and sub-THz frequencies, in order to assess its reliability, usability, and accuracy in practical cases. Results are compared with good results to estimates found in the literature for a set of reference materials.

The rest of the paper is organized as follows. The FP method is described in detail in section 2, including the new improvements to it. The method is checked versus reference literature results, and its applicability limitations are discussed in section 3. The method is finally applied to several materials and frequencies, including sub-THz frequencies in section 4, where results are summarized in Table 6, and conclusions are drawn in section 5.

2. Description of the Method

Electromagnetic characterization of materials consists in the determination of their complex relative permittivity $\varepsilon_r = \varepsilon' - j\varepsilon''$. We assume here that the imaginary part of ε_r is due to equivalent ohmic conduction, and therefore, $\varepsilon'' = \sigma/(2\pi f \varepsilon_0)$, where ε_0 is vacuum's permittivity. Applying the proposed method to low-loss materials, that is, with $\varepsilon'' \ll \varepsilon'$, real and imaginary parts can be determined separately in two steps, and therefore, the measurement procedure is simpler and less critical compared to traditional methods (Degli-Esposti et al., 2017; Possenti et al., 2020).

The first step in the measurement procedure is to determine the real part (ε') of the permittivity through the FP method (Degli-Esposti et al., 2017; Possenti et al., 2019, 2020); see section 2.3 for details. The FP mechanism can be outlined as follows: When a plane wave impinges on an infinite low-loss dielectric slab, a resonant phenomenon takes place due to a series of multiple reflections—and transmissions—within the slab. This phenomenon results in a frequency response pattern with a number of deep notches: the FP resonances (see, e.g., Figure 4a). By measuring the reflectivity of the slab for a given incidence angle over a wide-enough bandwidth B in order to highlight at least two or three resonance notches, and estimating the frequency distance Δf between two adjacent notches, it is possible to compute ε', according to the following equation (Degli-Esposti et al., 2017):

$$\varepsilon' = \left(\frac{c}{\Delta f \cdot 2w}\right)^2 + (\sin \vartheta_i)^2 \qquad (1)$$

where w (m) is slab thickness, ϑ_i (rad) is the incidence angle with respect to the surface normal, and c (m/s) is the speed of light. As the other quantities in Equation 1 are derived from the setup, once Δf is known, it is possible to estimate the value of ε', in the chosen bandwidth. It is worth noting that the higher the number of notches, the better the $\boldsymbol{\Delta f}$ estimation. If material characteristics—and therefore Δf—change over the measurement bandwidth B, the estimated ε' it is to be understood as a mean value over B. In the new, improved version of the method Δf estimation is performed through a spectral analysis (see section 2.2).

The second step is the evaluation of ε'' separately, through a transmission method by matching the measured transmission coefficient with a reference model (Possenti et al., 2019); see section 2.3 for details. A procedure has been developed to fit the theoretical model to a least squares approximation of the measured curve. The procedure leads to an estimate of the transmission loss of the slab over the considered bandwidth, using the ε' value previously estimated through Equation 1. Again, as the procedure provides only one value of σ, it has to be considered as a mean value over B.

Time gate filtering techniques (section 2.4) can be applied before the estimation of both ε' and ε'' in order to filter out environment multipath and noise. In ε' estimation, however, time gating must be limited in order to allow the FP resonance interference pattern to show up (see section 2.4).

2.1. Description of the Setup

Measurements have been performed through both a VNA (Figure 1), and a Spectrum Compact Analyzer (SCA) portable equipment (Figure 2) (SAF Tehnika, 2019).

Each equipment shows pro's and con's with respect to the performed measurement. Desktop VNA provides greater measurement capabilities and accuracies, but mobility is limited due to cables and instrument's size, which could be a relevant issue for some applications. On the other hand, SCA is a light, portable and easy-to-use measurement kit, useful for on-site measurements even of walls or furniture, but at the cost of a lower sensitivity and resolution.

For both cases the setup is exemplified in Figure 3: For reflection measurements (a), antennas are set symmetrically at a fixed incident angle with respect to the normal of the material under test (MUT)'s surface. As described in section 3.3 we used an incidence angle of $\vartheta_i = \pi/4$ rad. An absorber can be used to block the direct path between the antennas, though the procedure is resilient to crosstalk issues. For transmission measurements (b), antennas are set to be in front of each other. The transmission coefficient is computed by deembedding antenna gains and free space loss: To this aim, it is required to normalize the VNA output ($S_{21}^{MUT}(f)$) with a reference measurement, which is recorded keeping the two antennas in Line Of Sight (LOS) without the MUT in between ($S_{21}^{Freespace}(f)$). The transmission coefficient is then given by $\left|S_{21}^{MUT}(f)\right|/\left|S_{21}^{Freespace}(f)\right|$. It is worth noting that this normalization is not needed for reflection measurements.

In order to properly apply the FP method, some precautions must be taken during the setup. First of all, the slab's size should be large enough to ensure that the antenna's -3 dB lobe footprint is concentrated around the slab center to reduce edge diffraction effect, which might generate similar frequency oscillations as the FP resonance. Second, the distance between the slab and the aperture of the antennas should be at least at least 10–15 wavelengths to ensure far-field conditions. We set the transmitter and the receiver at a distance of 40 cm from the MUT for all setups. The dimensions of the horn should not be of concern given that horn antennas already generate a wavefront with quasi-far-field characteristics at the aperture of the horn with very small diffraction (Colin, 1985). Moreover, the slab should be uniform and flat with constant thickness in order to avoid lens effects. Finally, the frequency resolution should be high enough to identify unambiguously the position of the notches.

2.2. Estimation of ε'

The value of Δf to be used in Equation 1 might be estimated straight from the frequency response graph, but such a procedure is subjective, not very precise and problematic when noise and scattering generated by material's inhomogeneities blur the pattern and FP notches are not univocally identifiable (e.g.,
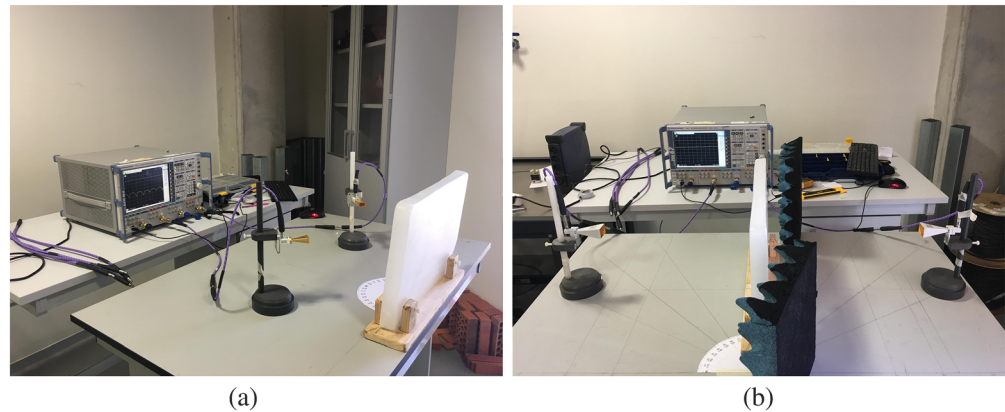
(a)   (b)

Figure 1. Measurement setup for (a) reflection and (b) transmission.

Figure 4b). In very inhomogeneous materials FP resonance does not take place and therefore the method cannot be applied. Therefore, an automated procedure based on a spectral analysis is defined in the following to solve the aforementioned problems. The procedure is based on the frequency response, that is, the absolute value of the measured response $|S_{21}(f)|$, which is FFT transformed to find the first harmonic (in the FFT-transformed time domain) corresponding to the resonance period Δf. The main purposes of the FFT-based procedure are (i) to understand if the FP resonance is actually established, (ii) if so, to estimate the correct resonance harmonic, and (iii) to estimate the quality of such a resonance.

In Figure 4, for example, paraffin (Figure 4a) shows a very clear periodic pattern, which translates into a prominent harmonic in the FFT-transformed spectrum, while chipboard (Figure 4b) does not shows a well-defined periodicity and the spectrum presents two main harmonics (red and blue lines). The black line in Figure 4 sets the lower bound for the acceptable FP harmonics as defined below, so that the first harmonic identified by the red line in Figure 4b must be discarded).

In order to identify the correct spectral component, it is worthwhile to find a range for acceptable Δf values. Recalling Equation 1, the value of ε' cannot be smaller than the value of the vacuum; therefore, $\varepsilon' \geq 1$. If $(\sin\vartheta_i)^2 = a$, with $\vartheta_i \in (0, \pi/2)$, we have
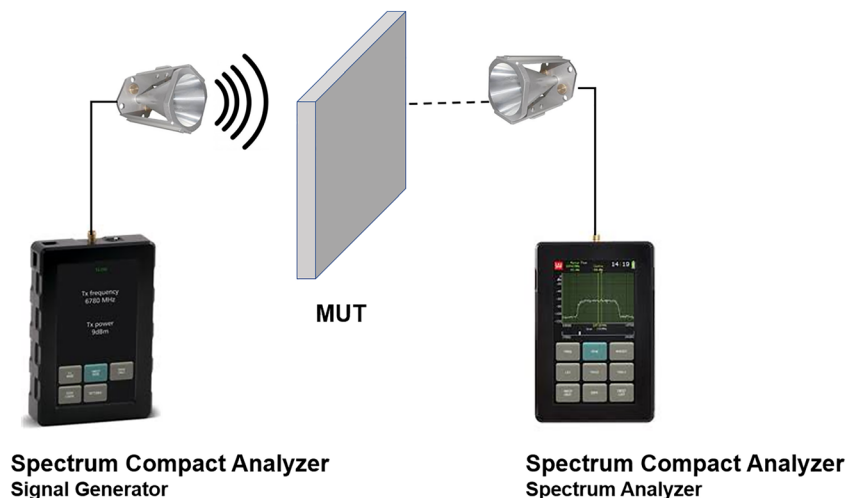

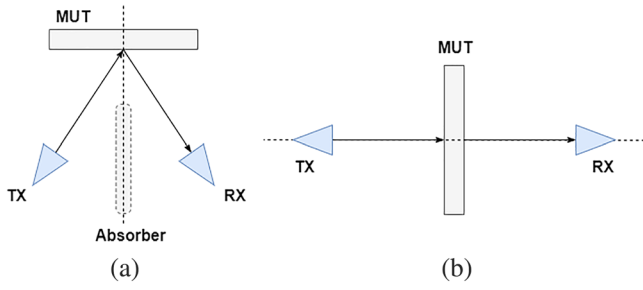**Figure 2.** Sketched measurement setup for transmission for SCA.

Figure 3. (a) Reflection measurement setup and (b) transmission measurement setup.

$$\left(\frac{c}{\Delta f \cdot 2w}\right)^2 \geq 1 - a \tag{2}$$

Hence,

$$\Delta f \cdot w \leq \frac{c}{2\sqrt{1-a}} \tag{3}$$

In Figure 5 the allowed range for $(\Delta f, w)$ pair is shown, for $\vartheta_i = [2\pi/9, \pi/3]$ rad. Given w, it is possible to check if the computed Δf value is meaningful.

In addition, if a range of reasonable "initial guess" values can be assumed for ε', for example, from values at other frequencies, literature, and so forth, it is possible to define the corresponding Δf range. If $\varepsilon'_{min} < \varepsilon' < \varepsilon'_{max}$, it must be

$$\frac{c}{2\sqrt{\varepsilon'_{max} - a}} \leq \Delta f \cdot w \leq \frac{c}{2\sqrt{\varepsilon'_{min} - a}} \tag{4}$$
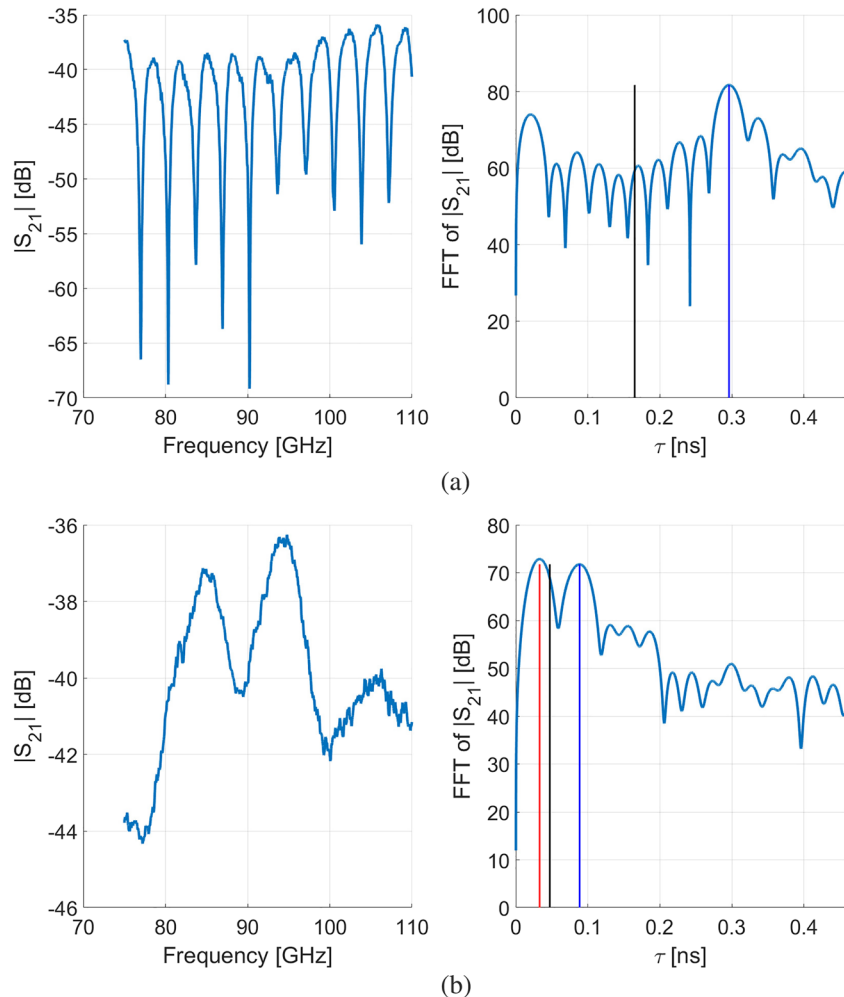

Figure 4. Frequency response patterns and their relative spectrum in two different cases: (a) a clear case of resonance for paraffin and (b) an ambiguous one for chipboard-3 (b).
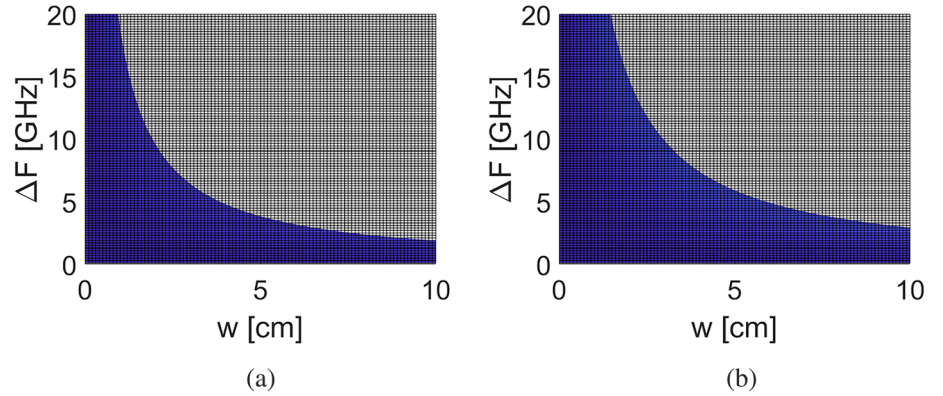
Figure 5. Regions for allowed $(\Delta f, w)$ pairs in blue, as a function of $\boldsymbol{a}$: (a) $\vartheta_i = 2\pi/9$ rad; (b) $\vartheta_i = \pi/3$ rad; In this example $\Delta f = 0.1 \div 20$ GHz and $w = 0.1 \div 10$ cm.

In order to assess if the FP resonance actually takes place, a comparison of the amplitudes of the frequency response's harmonics in the valid Δf range is performed: If the strongest harmonic is at least 3 dB above the second strongest harmonic, the resonance is confirmed; otherwise, if there are two (or more) harmonics with comparable amplitudes (i.e., within 3 dB), we are not able to solve the ambiguity and to determine which is the true resonance's harmonic. Moreover, it is clear that a minimum of two notches within the considered measurement bandwidth B is required in order to identify at least one Δf. Hence, it must be true that $\Delta f \leq B$. However, a stricter condition is necessary in order to ensure that FP resonance is good enough to yield reliable results. A number N of notches of the frequency response (see Figure 4) is required. Therefore, if a valid harmonic is found, as a final validity check, it must be $\Delta f \leq B/(N-1)$. A reasonable value for N is 4.

Finally, to estimate the quality of the occurred resonance (if any), we consider the quality factor Q, defined as the ratio between the resonance peak τ_0 and the resonance width $\Delta\tau$:

$$Q = \frac{\tau_0}{\Delta\tau} \qquad (5)$$

As shown in Figure 6, τ_0 is the blue line x axis position and $\Delta\tau$ is defined as the span between the half-power (black, dashed line) points of the resonance peak (red solid lines). The smaller the $\Delta\tau$ (hence, the higher Q), the better the resonance, as the harmonic is clearer.

As an example, $\Delta\tau$ for the two cases of Figure 4 are 0.0247 ns for the paraffin ($\tau_0 = 0.2960$ ns) and 0.0288 ns for the chipboard ($\tau_0 = 0.0885$ ns), leading to $Q = 12.00$ and $Q = 3.07$, respectively.
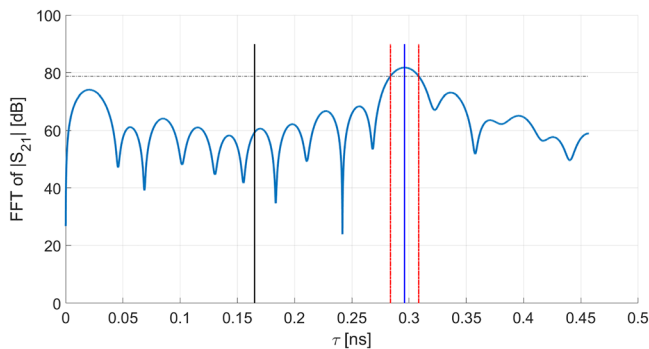
2.3. Estimation of ε''

Once ε' has been determined, ε'' must be estimated from the measurement of the transmission coefficient $T^{meas}(f)$ over the considered bandwidth. A proper procedure is applied by comparing a simulated transmission coefficient $T^{sim}(\sigma, f)$ and the measured transmission coefficient $T^{meas}(f)$ to determine the σ value—and therefore the ε'' value—that best matches the two. If hard time gating is applied, that is, FP resonance is cut off and transmission coefficients are constant in frequency (see section 2.4 below) or if the noise level is high, $T^{sim}(\sigma)$ should be computed using the single-path transmission formula in the Appendix A. Otherwise, the coefficients must be considered frequency dependent; the formula in Possenti et al. (2020) should be used to compute $T^{sim}(\sigma, f)$, and a frequency response pattern matching procedure must be adopted to determine the best fit σ. The problem can be stated as follows: find σ^{opt} such that
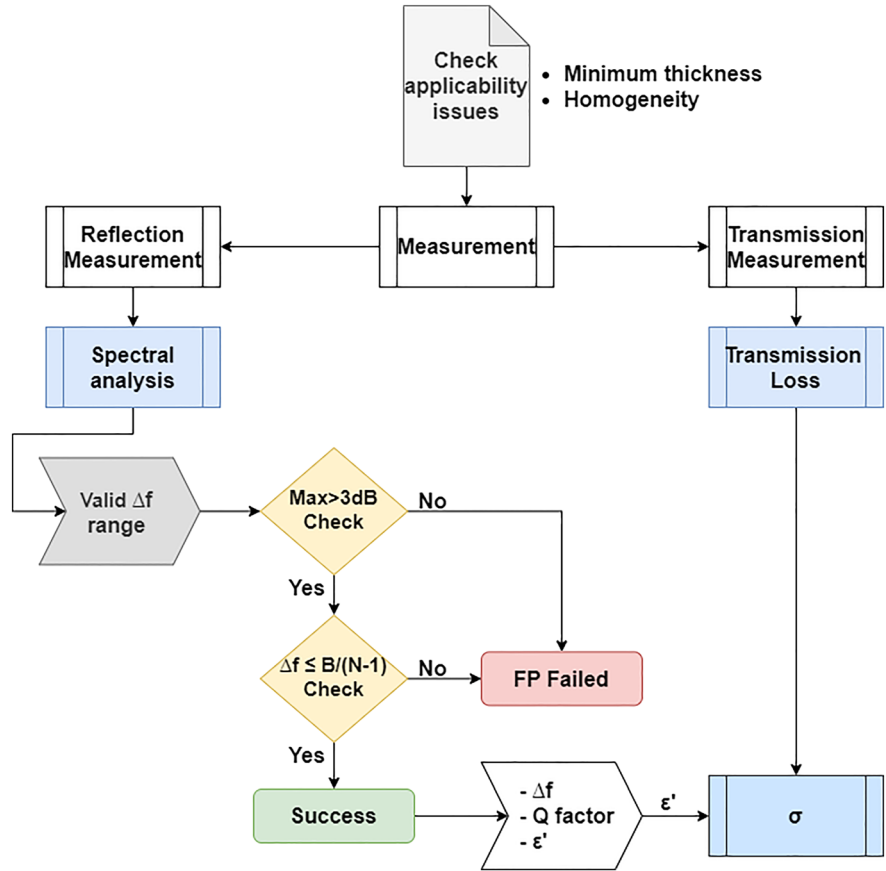

Figure 6. Paraffin (Figure 4a) resonance width $\Delta\tau$. The dashed black line is the -3 dB level under the maximum (blue line). The interval between these two points (red lines) is $\Delta\tau$.

Figure 7. Fabry-Pérot procedure.

$$\sigma^{opt} = \underset{\sigma}{argmin}\left(RMSE(\sigma)\right) \tag{6}$$

with

$$RMSE(\sigma) = \sqrt{mean_f\left[e^2(\sigma,f)\right]}$$

$$e(\sigma,f) = abs\left(\left|T^{meas}(f)\right| - \left|T^{sim}(\sigma,f)\right|\right)$$

where $e(\sigma)$ is the error of the simulated versus measured transmission coefficient. Error minimization is carried out using a standard iterative procedure until the desired precision is achieved.

Figure 7 shows a diagram with the main steps of the overall FP parameter estimation procedure, including the determination of both ε' through the reflection measurement (branch on the left) and ε'' through the transmission measurement (branch on the right).

2.4. Time Gating

Using the VNA inverse FFT function, time gating techniques can be applied a posteriori to reflection and/or transmission measurements in order to select and keep only contributions arriving within a given maximum delay after the first one and filter out later arrivals, including the environment multipath (Possenti et al., 2020). However, internal reflections must not be filtered out for ε' measurements using the FP interference pattern. It is worth mentioning that there is no relation between the number of internal reflections and the frequency distance between two adjacent FP notches (Δf). As a matter of fact, to satisfy Equation 1, the following equation should hold (Degli-Esposti et al., 2017):
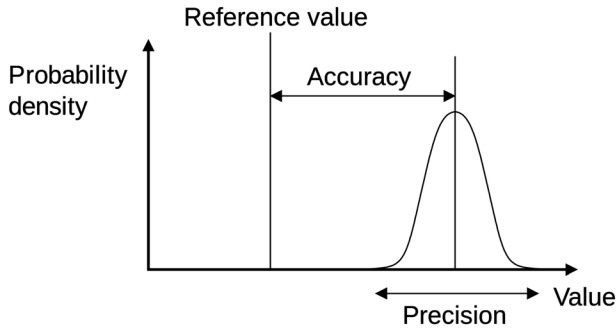
Figure 8. Accuracy and precision concepts.

$$\delta = \left(\frac{2\pi}{\lambda_0}\right) \cdot 2\sqrt{\varepsilon'} \cdot w \cdot \cos(\vartheta_T) = 2k\pi \qquad (7)$$

where δ is the phase rotation of the ith reflected component with respect to the $(i-1)$th one. As shown in Equation 7, δ does not depend on i, hence, the notches' position does not depend on the number of reflections retained within the time gate window, although a higher number of reflections can make notches deeper and more visible. Thus, it is enough to consider just two components (the direct path and the first double reflected path) in order for the interference pattern to show notches in the correct positions, thus allowing correct ε' measurements. With very simple geometric considerations on the double-reflected path, it is possible to show that the minimum time gate span (relative to the first arrival, direct path) to preserve the FP notches is

$$\Delta t_{\min} = \frac{2w}{\cos(\vartheta_T)} \cdot \frac{\sqrt{\varepsilon'}}{c} \qquad (8)$$

with obvious meaning of the symbols. Based on a conservative estimate of ε', the minimum time gate can be a priori determined using Equation 8.

Based on these evaluations, an "aggressive" time gating (hard time-gating) can be applied to single-out only the direct path in transmission measurements where—unlike reflection measurements—the FP resonance is not functional to the estimation procedure. By doing so, all the multipath interference and even the FP resonance ripple can be eliminated; the transmission coefficient becomes constant in frequency and its average value over the considered bandwidth can be considered, thus averaging out noise and using Equation 20 in the Appendix A to evaluate σ. However, if c is vacuum light speed and n is the refraction index, the delay of the first internal double reflection with respect to the direct path in case of normal incidence is

$$\Delta t = \frac{2w\,n}{c} \qquad (9)$$

Using the typical values $w = 4$ cm, and $n = 3$, we get $\Delta t = 0.8$ ns, which is below the time resolution of most setups. In the present work we used hard time gating to evaluate σ whenever possible, depending on the setup.

2.5. Pro's and Con's of the FP Method

As common materials are often heterogeneous compounds, they exhibit large variability between different samples and an accurate characterization is hardly possible. Rather than accuracy, simplicity, speed of execution, and the possibility of performing contactless and nondestructive measurement of large material samples are important features here. Under this perspective, an advantage of the FP method is that all measurements can be easily performed in one single shot without the need of multiple measurements for different incidence angles that would require rotating positioners and anechoic or quasi-anechoic conditions. The method only requires a simple, fixed measurement setup and the use of a general purpose VNA or SCA without the need of extensive calibration. Moreover, as stated in section 2.1 references are not required for reflection measurements as the relative distance between frequency domain notches, rather than absolute values of the reflection coefficient, is used for the estimate.

The main limit of the FP method resides in its applicability, which is limited to low-loss and flat materials. However, this requirement is common to several other characterization methods.

3. Validation

In order to understand the effectiveness of the method, accuracy and precision are two important factors to consider when dealing with data measurements. Accuracy refers to the closeness of the measurements to the

Table 1
Impact on the ε′ Estimate of Δf, ϑ$_i$, and w Errors

	Error on Δf ±10 MHz	Error on ϑ_i ±π/180	Error on w ±1 mm	Total
Error on ε'	0.56%	0.53%	5.65%	5.70%

Table 2
Relation Between Wavelength and Grain Size at FP Cutoff Frequency

	Cutoff frequency estimate	Wavelength	Mean grain size estimate
Wood	20 GHz	1.500 cm	0.33λ
Chipboard	80 GHz	0.375 cm	0.26λ
Granite	70 GHz	0.430 cm	0.28λ

true value. Precision is the degree to which repeated and reproduced measurements yield the same results, which turns into the spreading of measurements, as shown in Figure 8.

Moreover, the applicability of the method to different materials and cases has to be evaluated.

3.1. Accuracy

Measurements setup is subject to different errors which may come from:

a. The variation of the nominal (unknown) value of Δf, due to noise, VNA's resolution, FFT procedure resolution, and so forth;
b. The nonperfect alignment of the antennas to the nominal reflection and transmission angles of incidence together with the nonperfect perpendicularity of the slab to the leaning surface, which affect ϑ_i;
c. The nonperfect flatness of the slab, which would result in a slight variation of the thickness along the surface that must be considered as an error on w dimension.

In order to assess the FP accuracy, the impact of such errors on the real part of the complex permittivity is evaluated. To this aim, error propagation on Δf, ϑ_i, w, and ε' is analyzed.

Given a function of n uncorrelated variables x_i, $g(x_1, x_2, ...x_n)$, each affected by its uncertainty Δx_i ($x_i \pm \Delta x_i$), the uncertainty on $g(x_1, x_2, ...x_n)$, can be calculated as follows:

$$\Delta g = \sqrt{\sum_{i=1}^{n} \left(\frac{\delta g}{\delta x_i} \Delta x_i \right)^2} \tag{10}$$

In our case the target function g corresponds to the ε', given by Equation 1, while the error-affected variables (x_i) are Δf, ϑ_i, and w. Table 1 shows the relative error on ε' as a function of the three sources of error, separately computed using Equation 10, and the total error. Results are computed for $\Delta f = 3$ GHz, $\vartheta_i = \pi/4$ rad, and $w = 3$ cm.

3.2. Precision

Precision is a measure of the spreading of the values around the mean, and it is declined in repeatability and reproducibility.

As mentioned in section 2.1, we tested the FP approach also with the SCA kit. In (Possenti et al., 2019) the comparison between the two different setups is reported, showing a good agreement.

Different measurements performed on the same materials at the same frequency are shown to get a grasp of the precision of the method. As shown in section 4, the precision is good although they have been conducted in different moments, by different operators and with different VNAs, and even in two different labs (in Italy and in Spain). For example, the same paraffin slab has been tested under different conditions at 10 GHz, and
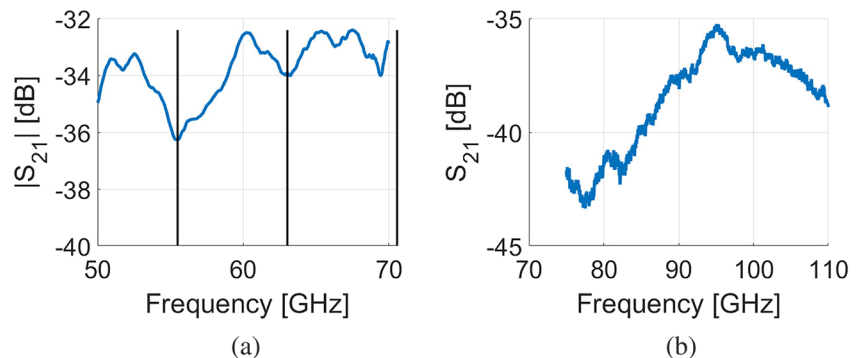

Figure 9. Working (a) and failing (b) bands for a chipboard slab. Black solid lines in (a) highlight the notches' position ($\Delta f = 7.53$ GHz).

Table 3
Marble's results at 30 GHz for Three Different Incidence Angles

	Δf (GHz)	ε'
$\vartheta_i = \pi/6 \text{rad}$	1.824	7.561
$\vartheta_i = \pi/4 \text{rad}$	1.883	7.563
$\vartheta_i = \pi/3 \text{rad}$	1.893	7.564

results are in very good agreement (see section 4 and Table 6). Granite has been tested in different conditions at 60 GHz, showing good agreement as well (see section 4 and Table 6).

3.3. Applicability

There are some aspects that should be considered for the FP applicability.

First of all, it is worthwhile to know a priori an approximate minimum thickness of the slab for observing at least three to four adjacent notches, which is related to the measurement bandwidth B. In order to highlight N notches, it must be $\Delta f \le B/(N-1)$. From Equation 4 we can extract a lower bound for the thickness:

$$w_{min} = \frac{c \cdot (N-1)}{2B \cdot \sqrt{\varepsilon'_{max} - a}} \tag{11}$$

From Equation 11 it is clear that the lower B the higher w_{min}. Figure 5 of section 2.2 shows the valid region for Δf for a given value of thickness w. Such value must be greater than w_{min} according to the measurement bandwidth B. For example, the minimum thickness for a brick at $B = 5$ GHz is $w_{min} = 2.92$ cm (considering $\varepsilon'_{max} = 10$, $N = 4$ and $\vartheta_i = \pi/4$ rad).

Moreover, although "grainy," inhomogeneous materials can be measured with the FP method as long as the wavelength is much larger than the average grain size, at high frequencies inhomogeneity could generate diffuse scattering and prevent the resonance from taking place. It is interesting to roughly estimate the cutoff frequency at which the FP resonance ceases to exist as frequency increases: Table 2 shows the cutoff frequency for some inhomogeneous materials. Figure 9 shows examples of reflection frequency responses for a working band (around 60 GHz) and a failing band (around 100 GHz) for chipboard.

Although we did not carry out a thorough investigation on this point, there seems to be a fixed ratio of about 0.3 between the size of grains and the wavelength at the cutoff frequency.

Table 4
ε' Estimates for brick, Teflon, Paraffine, and Sandstone: FP Method (Bold Character) Versus Literature

	4–60 GHz	70–100 GHz	200–300 GHz
Brick	**5.64 (30 GHz)** **5.32 (60 GHz)** 3.70–4.48 (4–40 GHz) (Abel & Wallace, 2019) 4.11 (18 GHz) (Stavrou & Saunders, 2003) 3.7–4 (9–24 GHz) (Stavrou & Saunders, 2003) 4.11–4.46 (2–40 GHz) (Ferreira et al., 2014) 3.95–4.41 (60 GHz) (Ferreira et al., 2014)		
Teflon		**2.22 (100 GHz)** 2.043 (122–169 GHz) (Alawneh et al., 2019) 2.05 (68–92 GHz) (Alawneh et al., 2019) 2.05 (100 GHz) (Hirvonen et al., 1996)	**2.25 (300 GHz)** 2.064–2.190 (207–247 GHz) (Alawneh et al., 2019) 2.061–2.069 (100–300 GHz) (Afsar, 1987) 2.107 (300 GHz) (Kazemipour et al., 2015) 2.06 (300 GHz) (Chang et al., 2017) 2 (50–500 GHz) (Kazemipour et al., 2015)
Paraffin	**2.03 (10 GHz)** 2.2–2.4 (10 GHz) (Von Hippel, 1966)		**2.19 (300 GHz)** 2.248–2.283 (300GHz-1THz) (Ghassemiparvin & Ghalichechian, 2016)
Sandstone	**7.7 (10 GHz)** **6.53 (30 GHz)** 5.37–5.64 (1.1–1.7 GHz) (Vaccaneo et al., 2004)		
Pine wood	**2.10 (10 GHz)** 2 (10 GHz) (Zhekov et al., 2020)		

Table 5
σ Estimates for Brick, Teflon, Paraffine, and Sandstone: FP Method (Bold Character) Versus Literature

	4–40 GHz	70–100 GHz	200–300 GHz
Brick	**0.13 (30 GHz)** **0.27 (60 GHz)** 0.036 (18 GHz) (Stavrou & Saunders, 2003) 0.04–0.8 (9–24 GHz) (Stavrou & Saunders, 2003)		
Teflon		**$4.48 \cdot 10^{-3}$ (100 GHz)** $2.6 \cdot 10^{-3}$ (100 GHz) (Hirvonen et al., 1996)	**$5.86 \cdot 10^{-3}$ (300 GHz)** $4.75 \cdot 10^{-4}$ (300 GHz) (Kazemipour et al., 2015) $1.6 \cdot 10^{-2}$ (280 GHz) (Afsar, 1987) $6.4 \cdot 10^{-2}$ (280 GHz) (Chang et al., 2017) 0.16 (50–500 GHz) (Kazemipour et al., 2015)
Paraffin	**$2.6 \cdot 10^{-4}$ (10 GHz) $8.17 \cdot 10^{-3}$ (30 GHz)** 2.4–$2.8 \cdot 10^{-4}$ (10 GHz) (Von Hippel, 1966)		**0.04 (100 GHz, 300 GHz)** 0.01–0.9 (300 GHz-1THz) (Ghassemiparvin & Ghalichechian, 2016)
Sandstone	**0.09 (10 GHz)** **0.25 (30 GHz)** 0.012–0.022 (1.1–1.7 GHz) (Vaccaneo et al., 2004)		
Pine wood	**0.07 (10 GHz)** 0.078 (10 GHz) (Zhekov et al., 2020)		

Another applicability issue, actually common to many other methods, is that for very low conductivity materials the measured transmission coefficient may approach 1, making the estimation of ε'' or σ challenging.

It is worth noting that ε' results are virtually independent of the chosen incidence angle ϑ_i, as shown in Table 3. However, as diffraction on the slab's vertical edges might arise with very large angles, while the antennas could get too close to each other for very small angles and crosstalk effect may corrupt measurements, we decided to use the intermediate angle value $\vartheta_i = \pi/4$ rad.

3.4. Validation Versus Reference Results

Validating measurement methods for material parameters is a quite difficult task. While there is a vast literature on such methods, only in very few cases the error or the confidence level of the measured parameter values is provided (Abel & Wallace, 2019; Afsar, 1987; Alawneh et al., 2019; Chang et al., 2017; Ferreira et al., 2014; Ghassemiparvin & Ghalichechian, 2016; Hirvonen et al., 1996; Kawabata et al., 2006; Kazemipour et al., 2015; Krupka, 2016; Stavrou & Saunders, 2003; Von Hippel, 1966). Moreover, common materials are inhomogeneous and vary quite a lot with the manufacturing method, even between different samples for the same manufacturer. For this reason, we decided to validate the FP method using reference low-loss materials often used in constructions and in the industry, namely, brick-clay, teflon (PTFE), paraffin, sandstone, and pine wood, for which some reliable data are available in the literature.

The following Tables 4 and 5 compare FP estimates (in bold) with values found in the literature for similar frequency bands.

Values in Table 4 (ε') are in good agreement with FP measurements, the error being always below 10% for teflon and paraffin. The error is larger for brick clay. However, brick material is known to be highly variable: We used a relatively thin and dense clay tile used for floor coating, while brick clay for wall construction is usually considered in the literature. It is worth noting that even teflon is quite variable: Besides polytetrafluoroethylene (PTFE) considered in the present work, it can also be perfluoroalkoxy alkane (PFA) or fluorinated ethylene propylene (FEP) that have a slightly different composition: Unfortunately, the exact composition is rarely indicated in the literature.

For σ values (Table 5) the order of magnitude is always matched by the FP method, while the exact estimate figure varies quite a lot, not only between FP and literature references but even between such different literature results. As stated before, this is partly due to the great variability of building materials (Stavrou & Saunders, 2003). But for very low loss polymers, where the grade of discrepancy can be even of 1 order of magnitude, the cause is probably the insufficient sensitivity of measurement methods used by researchers compared to the very low value of the loss tangent (Krupka, 2016).

Table 6
Fabry-Pérot Results

Frequency band (GHz)		8–13			26–40			50–70			75–110			220–330		
Bandwidth (GHz)		5			14			20			35			110		
		10 GHz			30 GHz			60 GHz			100 GHz			300 GHz		
Material	w (cm)	ε'	σ	L_T	ε'	σ	L_T	ε'	σ	L_T	ε'	σ	L_T	ε'	σ	L_T
Brick	1.5	w too small			5.64	0.13	2.92	5.32	0.27	5.71	5.57	0.36	9.28			
Chipboard-1	1.6	w too small			2.19	0.11	2.28	2.04	0.48	9.07			16.51			46.91
Chipboard-2	1.6	w too small			2.15	0.12	2.46	1.85	0.41	8.09			11.94			45.29
Chipboard-3	1.0	w too small			5.66	0.12	2.41	4.93	0.92	8.12			10.73			18.82
Chipboard-4	2.0	2.60	0.15	3.54	2.60	0.26	5.76									
Granite	2.1							5.51	0.42	7.13			18.51			
								5.53	0.40	7.10			18.04			
Plaster	2.0	w too small					8.02			10.88	1.71					10.97
Marble	3.0	6.90	0.15	4.75	7.56	0.06	3.21									
Nylon	0.6	w too small			w too small			w too small			3.95	0.13	1.65	3.86	0.66	4.27
Paraffin*	3.5	2.00	0.23e-3	0.27	2.25	8.17e-3	0.67	2.36	0.03	1.51	2.11	0.04	1.87	2.19	0.04	1.88
Paraffin**	3.5	2.03	0.26e-3	0.30												
Pine wood	4.5	2.10	0.07	3.85			14.33									
Plywood	1.8			2.25	1.77	0.21	4.82	1.81	0.44	9.82			17.11			38.06
Sandstone	3.0	7.70	0.09	3.76	6.53	0.25	6.64									
Teflon	1.0	w too small			w too small			w too small			2.22	4.48e-3	0.39	2.25	5.86e-3	0.42
Tile	0.7	w too small			6.27			5.88	0.59	4.44			4.72			12.88

4. Application Results

In this section we present the overall results of the FP procedure in terms of ε' and σ (S/m) for the considered reference materials. Results are shown in Table 6, also including the insertion loss L_T (dB). As can be noted, some materials could not be measured at lower frequencies because thickness of samples w was too small given the considered frequency band (see Equation 11), as highlighted in the table. As mentioned in section 3.2, the same paraffin slab has been tested with two different measurement setups (see Paraffin* and Paraffin**), in two different labs and results are in very good agreement with each other.

Gray cell means that no data are available for that case, as no measurements were performed. In green cells FP procedure worked properly. Finally, in red cells, FP failed, due to one of the two checks not being satisfied (see section 2.2) or to applicability issues as highlighted in the flow chart of Figure 7. However, even in this case, the average transmission (or insertion) loss L_T could be estimated and therefore it has been reported in the third column of each frequency band: This is a useful side result of the FP measurement procedure.

Values reported in Table 6 are in good agreement with those reported in the literature for similar materials and frequencies (Rappaport et al., 2019; Stavrou & Saunders, 2003; Von Hippel, 1966). The conductivity appears to be increasing with frequency for almost all materials, in agreement with the frequency-dependent formula suggested by ITU (International Telecommunication Union, 2015). Interestingly, marble represents an exception to the rule, confirming what was already found in Degli-Esposti et al. (2017).

5. Conclusions

The FP method recently proposed for the electromagnetic characterization of common construction and furniture materials has been improved and applied to several materials at mm-wave and sub-THz frequencies, in order to assess its reliability, usability, and accuracy in practical cases. Different setups, including a portable SA for on-site measurements have been used to show the flexibility of the method. Interesting results for several different common use materials have been obtained at several mm-wave and sub-THz frequencies. While the application of the method to sub-6 GHz frequencies would require too thick material

samples and at THz frequencies would suffer in case of grainy materials with grain dimension comparable to, or larger than, the wavelength, the method appears quite suitable for mm-wave and sub-THz frequencies. A good accuracy level is achieved with a very basic setup and a fast measurement procedure. Some application limitations are highlighted and discussed. For the last word on accuracy, the method will have to be applied multiple times to more material samples of certified characteristics or will have to be compared with reference methods of certified precision and accuracy for the same material samples. This will be the object of future work.

Appendix A: Insertion Loss Formula for a Low-Loss Slab

In the following we derive an approximate, simple formula for the estimation of single-path transmission loss through a dielectric, low-loss slab. Assumptions are as follows:

a. normal incidence
b. low-loss material with $\varepsilon'' \ll \varepsilon'$
c. single transmitted path undergoing two reflections (on the air-to-medium and medium-to-air interfaces) and attenuation through the slab material

The wavenumber of the low-loss material with $\varepsilon'' \ll \varepsilon'$ and $\mu = \mu_0$ can be simplified as follows:

$$k = \omega\sqrt{\mu_0\varepsilon_0}\sqrt{\varepsilon'-j\varepsilon''} = \frac{\omega}{c}\sqrt{\varepsilon'-j\varepsilon''} == \frac{\omega}{c}\sqrt{\varepsilon'}\sqrt{1-j\frac{\varepsilon''}{\varepsilon'}} \approx \frac{\omega}{c}\sqrt{\varepsilon'}\left(1-j\frac{\varepsilon''}{2\varepsilon'}\right) \tag{12}$$

where the last equality derives from Taylor's expansion truncated to the first term. Therefore, we can derive the expression of the attenuation constant α:

$$k = \alpha - j\beta \approx \frac{\omega}{c}\sqrt{\varepsilon'}\left(\frac{\varepsilon''}{2\varepsilon'}+j\right) \tag{13}$$

$$\alpha \approx \frac{\omega}{c}\sqrt{\varepsilon'}\left(\frac{\varepsilon''}{2\varepsilon'}\right) = \frac{\sigma}{2\varepsilon_0 c\sqrt{\varepsilon'}} \tag{14}$$

Note that α does not depend directly on frequency. It can be easily shown that Fresnel's TE and TM reflection coefficients are equal in case of normal incidence, and their expressions for the air-to-medium interface (Γ_{0m}) and at the medium-to-air interface (Γ_{m0}) are as follows:

$$\Gamma_{0m} = \frac{1-\sqrt{\varepsilon_r}}{1+\sqrt{\varepsilon_r}} = -\Gamma_{m0} \tag{15}$$

Let us now consider incident, reflected, and transmitted power densities at the first interface S_{i1}, S_{r1}, and S_{t1}. It must be:

$$S_{i1} = S_{r1} + S_{t1} \Rightarrow S_{t1} = S_{i1}\left(1-|\Gamma_{0m}|^2\right) \tag{16}$$

A similar equation holds for the second interface:

$$S_{t2} = S_{i2}\left(1-|\Gamma|^2\right) = S_{t1}e^{-2\alpha w}\left(1-|\Gamma|^2\right) = \\ = S_{i1}\left(1-|\Gamma|^2\right)e^{-2\alpha w}\left(1-|\Gamma|^2\right) \tag{17}$$

where α is the attenuation constant 13, and

$$|\Gamma| = |\Gamma_{0m}| = |\Gamma_{m0}| = \left|\frac{1-\sqrt{\varepsilon_r}}{1+\sqrt{\varepsilon_r}}\right| \tag{18}$$

because of 14. Therefore, the overall insertion loss is

$$L_T = \frac{S_{i1}}{S_{t2}} = \frac{e^{2\alpha w}}{\left(1 - |\Gamma|^2\right)^2} \tag{19}$$

Therefore, the transmission coefficient in dB can be computed as follows:

$$T[dB] = -10 \cdot Log(L_T) \tag{20}$$

Note that L_t and T depend on α and therefore ultimately on conductivity σ.

Data Availability Statement

The data are deposited in a public accessible domain and can be found in the link (https://figshare.com/articles/figure/Figure_zip/12608684).

References

Abel, J. R., & Wallace, J. W. (2019). 4–40 GHz permittivity measurements of indoor building materials. In *IEEE international symposium on antennas and propagation and USNC-URSI radio science meeting* (pp. 105–106). Atlanta, GA, USA. https://doi.org/10.1109/APUSNCURSINRSM.2019.8888911

Afsar, M. N. (1987). Precision millimeter-wave measurements of complex refractive index, complex dielectric permittivity, and loss tangent of common polymers. *IEEE Transactions on Instrumentation and Measurement*, *IM-36*(2), 530–536. https://doi.org/10.1109/TIM.1987.6312733

Alawneh, I., Barowski, J., & Rolfes, I. (2019). Measuring the permittivity of dielectric materials by using 140 GHz FMCW radar sensor. In *13th European conference on antennas and propagation (EuCAP)* (pp. 1–4). Krakow, Poland.

Boughriet, A., Legrand, C., & Chapoton, A. (1997). Non-iterative stable transmission/reflection method for lowloss material complex permittivity determination. *IEEE Transaction on Microwave Theory and Methods*, *45*(1).

Canós Marín, A. J., García-Baños, B., Catalá-Civera, J. M., Peñaranda-Foix, F. L., & Gutiérrez-Cano, J. D. (2013). Improvement in the accuracy of dielectric measurement of open-ended coaxial resonators by an enhanced De-embedding of the coupling network. *IEEE Transactions on Microwave Theory and Techniques*, *61*(12), 4636–4645. https://doi.org/10.1109/TMTT.2013.2285359

Chang, T., Zhang, X., Zhang, X., & Cui, H. (2017). Accurate determination of dielectric permittivity of polymers from 75 GHz to 1.6 THz using both S-parameters and transmission spectroscopy. *Applied Optics*, *56*(12), 3287–3292. https://doi.org/10.1364/AO.56.003287

Colin, R. E. (1985). *Antennas and radiowave propagation*. New York: McGraw Hill.

Cuong, H. M., Duc, N. T., & Van Yem, V. (2017). Measurement of complex permittivity of materials using electromagnetic wave propagation in free space and super high-resolution algorithm. In *International Conference on Advanced Technologies for Communications (ATC)* (pp. 156–160). Quy Nhon. https://doi.org/10.1109/ATC.2017.8167607

Degli-Esposti, V., Zoli, M., Vitucci, E. M., Fuschini, F., Barbiroli, M., & Chen, J. (2017). A method for the electromagnetic characterization of construction materials based on Fabry–Pérot resonance. *IEEE Access*, *5*, 24,938–24,943. https://doi.org/10.1109/ACCESS.2017.2767278

Elayan, H., Amin, O., Shihada, B., Shubair, R. M., & Alouini, M. (2020). Terahertz band: The last piece of RF spectrum puzzle for communication systems. *IEEE Open Journal of the Communications Society*, *1*, 1–32. https://doi.org/10.1109/OJCOMS.2019.2953633

Ferreira, D., Cuiñas, I., Caldeirinha, R. F. S., & Fernandes, T. R. (2014). A review on the electromagnetic characterisation of building materials at micro- and millimetre wave frequencies. In *The 8th European Conference on Antennas and Propagation (EuCAP 2014)* (pp. 145–149). The Hague. https://doi.org/10.1109/EuCAP.2014.6901713

Ghassemiparvin, B., & Ghalichechian, N. (2016). Permittivity and dielectric loss measurement of paraffin films for mmW and THz applications. In *2016 International Workshop on Antenna Technology (iWAT)* (pp. 48–50). Cocoa Beach, FL. https://doi.org/10.1109/IWAT.2016.7434797

Ghodgaonkar, D. K., Varadan, V. V., & Varadan, V. K. (1989). A free-space method for measurement of dielectric constants and loss tangents at microwave frequencies. *IEEE Transactions on Instrumentation and Measurement*, *38*(3), 789–793. https://doi.org/10.1109/19.32194

Ghodgaonkar, D. K., Varadan, V. V., & Varadan, V. K. (1990). Free-space measurement of complex permittivity and complex permeability of magnetic materials at microwave frequencies. *IEEE Transactions on Instrumentation and Measurement*, *39*(2), 387–394. https://doi.org/10.1109/19.52520

Hilario, M. S., Hoff, B. W., Jawdat, B., Lanagan, M. T., Cohick, Z. W., Dynys, F. W., et al. (2019). W-band complex permittivity measurements at high temperature using free-space methods. *IEEE Transactions on Components, Packaging and Manufacturing Technology*, *9*(6), 1011–1019. https://doi.org/10.1109/TCPMT.2019.2912837

Hirvonen, T. M., Vainikainen, P., Lozowski, A., & Raisanen, A. V. (1996). Measurement of dielectrics at 100 GHz with an open resonator connected to a network analyzer. *IEEE Transactions on Instrumentation and Measurement*, *45*(4), 780–786. https://doi.org/10.1109/19.516996

International Telecommunication Union (2015). Effects of building materials and structures on radiowave propagation above about 100 MHz, *Standard: ITU-R P.2040*, July 2015.

Kawabata, H., Hasuike, K., Kobayashi, Y., & Ma, Z. (2006). Multi-frequency measurements of complex permittivity of dielectric plates using higher-order modes of a balanced-type circular disk resonator. In *European Microwave Conference* (pp. 388–391). Manchester. https://doi.org/10.1109/EUMC.2006.281355

Kazemipour, A., Hudliˇcka, M., Yee, S., Salhi, M. A., Allal, D., Kleine-Ostmann, T., & Schrader, T. T. (2015). Design and calibration of a compact quasi-optical system for material characterization in millimeter/submillimeter wave domain. *IEEE Transactions on Instrumentation and Measurement*, *64*, 1438–1445.

Krupka, J. (2016). Measurements of the complex permittivity of low loss polymers at frequency range from 5 GHz to 50 GHz. *IEEE Microwave and Wireless Components Letters*, *26*(6), 464–466. https://doi.org/10.1109/LMWC.2016.2562640

Politiko, A. A., Semenenko, V. N., Chistyaev, V. A., & Baskov, K. M. (2019). Bench for measuring electromagnetic properties of materials in free space in a ultrawide microwave range. In *Radiation and scattering of electromagnetic waves (RSEMW)* (Vol. 2019, pp. 328–331). Russia: Divnomorskoe. https://doi.org/10.1109/RSEMW.2019.8792787

Possenti, L., Barbiroli, M., Degli-Esposti, V., Fuschini, F., & Vitucci, E. M. (2019). E.M. characterization of common construction materials using the Fabry-Pérot resonance method. In *International Symposium on Antennas and Propagation (ISAP)* (pp. 1–3). Xi'an, China.

Possenti, L., García, J. P., Degli-Esposti, V., Lozano-Guerrero, A., Barbiroli, M., Martinez-Inglés, M. T., et al. (2020). Transmission loss evaluation for Fabry-Perot materials' characterization. In *14th European Conference on Antennas and Propagation (EuCAP 2020) Copenhagen*, Denmark.

Rao, B. R. (1989). Free-space millimeter-wave measurement of the complex dielectric constant of radome materials using nonlinear least-squares analysis. In *Digest on Antennas and Propagation Society International Symposium* (Vol. 3, pp. 1534–1537). San Jose, CA, USA. https://doi.org/10.1109/APS.1989.135014

Rappaport, T. S., Xing, Y., Kanhere, O., Ju, S., Madanayake, A., Mandal, S., et al. (2019). Wireless communications and applications above 100 GHz: Opportunities and challenges for 6G and beyond. *IEEE Access*, 7, 1.

Redheffer, R. M. (1947). The measurement of dielectric constants. In *Technique of microwave measurements*. New York, NY, USA: McGraw-Hill.

SAF Tehnika Spectrum Compact Analyzer [Reference Manual] (2019). Retrieved from https://www.saftehnika.com/en/spectrumanalyzer

Salous, S., Degli Esposti, V., Fuschini, F., Dupleich, D., Müller, R., Thomä, R. S., et al. (2016). Millimeter-wave propagation characterization and modelling towards 5G systems. *IEEE Antennas and Propagation Magazine*, *58*(6), 115–127. https://doi.org/10.1109/MAP.2016.2609815

Stavrou, S., & Saunders, S. R. (2003). Review of constitutive parameters of building materials. In *Twelfth International Conference on Antennas and Propagation, 2003 (ICAP 2003)* (Conf. Publ. No. 491, Vol. 1, pp. 211–215). Exeter, UK. https://doi.org/10.1049/cp:20030052

Vaccaneo, D., Sambuelli, L., Marini, P., Tascone, R., & Orta, R. (2004). Measurement system of complex permittivity of ornamental rocks in L frequency band. *IEEE Transactions on Geoscience and Remote Sensing*, *42*(11), 2490–2498. https://doi.org/10.1109/TGRS.2004.835225

Von Hippel, A. R. (1966). *Dielectric materials and applications*. Boston: Artech House Microwave Library.

Works, C. N., Dakin, T. W., & Boggs, F. W. (1944). A resonant-cavity method for measuring dielectric properties at ultrahigh frequencies. *Transactions of the American Institute of Electrical Engineers*, *63*(12), 1092–1098. https://doi.org/10.1109/T-AIEE.1944.5058852

Zhekov, S. S., Franek, O., & Pedersen, G. F. (2020). Dielectric properties of common building materials for ultrawideband propagation studies [measurements corner]. *IEEE Antennas and Propagation Magazine*, *62*(1), 72–81. https://doi.org/10.1109/MAP.2019.2955680